Molecular Pharmacology Fast Forward. Published on April 29, 2015 as DOI: 10.1124/mol.114.096792
This article has not been copyedited and formatted. The final version may differ from this version.

ABC Transporter Structure Changes Detected by Intramolecular Fluorescence Energy Transfer for High-throughput Screening

Surtaj H. Iram, Simon J. Gruber, Olga N. Raguimova, David D. Thomas, and Seth L. Robia

Department of Cell and Molecular Physiology, Stritch School of Medicine, Loyola University Chicago, Maywood, IL, USA. (S.H.I., O.N.R., S.L.R.)

Cardiovascular Research Institute, Stritch School of Medicine, Loyola University Chicago, Maywood, IL, USA. (O.N.R., S.L.R.)

Department of Biochemistry, Molecular Biology, and Biophysics, University of Minnesota, Minneapolis, MN, USA (S.J.G., D.D.T)

Department of Chemistry and Biochemistry, South Dakota State University, SD, USA (current address, S.H.I.)

To whom correspondance should be addressed: Seth L. Robia, Department of Cell and Molecular Physiology, Stritch School of Medicine, Loyola University Chicago, 2160 South First Avenue, Maywood, IL 60153, Tel: (708) 216-2522, E-mail: srobia@luc.edu

Molecular Pharmacology Fast Forward. Published on April 29, 2015 as DOI: 10.1124/mol.114.096792
This article has not been copyedited and formatted. The final version may differ from this version.

Running title: 2-Color Multidrug Resistance Protein

To whom correspondance should be addressed: Seth L. Robia, Department of Cell and Molecular Physiology, Stritch School of Medicine, Loyola University Chicago, 2160 South First Avenue, Maywood, IL 60153, Tel: (708) 216-2522, E-mail: srobia@luc.edu

Text Pages: 37

Tables: 0

Figures: 4

References: 60

Abstract: 188 words

Introduction: 907 words

Results and Discussion: 2707 words

List of Non-standard Abbreviations

ABC, ATP-binding cassette; MRP1, multidrug resistance protein 1; MSD, membrane spanning domain; NBD, nucleotide binding domain; NBS, nucleotide binding site; $E_2$17βG, 17β-estradiol-17-β-(D-glucuronide); DOX, doxorubicin; FRET, fluorescence resonance energy transfer; TIRF, total internal reflection fluorescence.

Molecular Pharmacology Fast Forward. Published on April 29, 2015 as DOI: 10.1124/mol.114.096792
This article has not been copyedited and formatted. The final version may differ from this version.

Abstract

Multidrug resistance protein 1 (MRP1) actively transports a wide variety of drugs out of cells. To quantify MRP1 structural dynamics, we engineered a "2-color MRP1" construct by fusing GFP and TagRFP to MRP1 nucleotide binding domains NBD1 and NBD2, respectively. The recombinant MRP1 protein expressed and trafficked normally to the plasma membrane. 2-color MRP1 transport activity was normal, as shown by vesicular transport of [^{3}H]$E_2$17βG and doxorubicin efflux in AAV-293 cells. We quantified fluorescence resonance energy transfer (FRET) from GFP to TagRFP as an index of NBD conformational changes. Our results show that ATP binding induces a large-amplitude conformational change that brings the NBDs into closer proximity. FRET was further increased by substrate in the presence of ATP, but not by substrate alone. The data suggest that substrate binding is required to achieve a fully closed and compact structure. ATP analogs bind MRP1 with reduced apparent affinity, inducing a partially closed conformation. The results demonstrate the utility of the 2-color MRP1 construct for investigating ABC transporter structural dynamics, and it holds great promise for high-throughput screening of chemical libraries for unknown activators, inhibitors, or transportable substrates of MRP1.

Molecular Pharmacology Fast Forward. Published on April 29, 2015 as DOI: 10.1124/mol.114.096792
This article has not been copyedited and formatted. The final version may differ from this version.

Introduction

The ATP-binding cassette (ABC) proteins comprise one of the largest superfamilies of membrane proteins and are ubiquitous in all forms of life. The ABC transporters can be classified as importers (bringing substrates into the cell) or exporters (expelling substrates from the cell). Both importers and exporters are present in prokaryotes whereas only exporters are found in eukaryotes. The importance of ABC transporters is highlighted by the fact that mutations in several members of the family are associated with human disease (Aittoniemi et al., 2009; Gottesman, 2002; Sheppard and Welsh, 1999). ABC proteins are capable of transporting a wide variety of xenobiotics, including organic anions from endogenous and exogenous sources, many of which are conjugated to GSH (e.g. cysteinyl leukotriene, LTC_4), glucuronide (e.g. estradiol glucuronide, $E_2$17βG), or sulfate (e.g. estrone sulfate, E_2SO_4) (Conseil et al., 2006; Deeley et al., 2006). This pan-specific export activity is relevant to clinical practice as it is the basis of physiological resistance to a wide variety of drugs. In particular, overexpression of ABC transporters such as P-glycoprotein (P-gp/ ABCB1), multidrug resistance protein 1 (MRP1/ABCC1) and breast cancer resistance protein (BCRP/ABCG2) may lead to failure of chemotherapy in cancer patients. These ABC transporters mediate ATP-dependent efflux of anti-cancer drugs across the plasma membrane leading to reduced intracellular accumulation and consequently reduced efficacy of those drugs.

The prototypical functional ABC transporter has a four-domain core structure, composed of two membrane spanning domains (MSDs) and two cytoplasmic nucleotide-binding domains (NBDs) (Dean and Allikmets, 2001). Available structural data suggest that the transmembrane (TM) α-helices of the two MSDs are intertwined to form the substrate translocation pathway and extend

Molecular Pharmacology Fast Forward. Published on April 29, 2015 as DOI: 10.1124/mol.114.096792
This article has not been copyedited and formatted. The final version may differ from this version.

into the cytoplasm making contacts with the NBDs (Hollenstein et al., 2007). Several ABC transporters, including MRP1, have an additional MSD (MSD0) at the amino-terminus of the protein. (Fig. 1A) (Hipfner et al., 1997). The precise function of MSD0 is not yet fully understood. Structural studies of bacterial ABC transporters captured in a state reflecting ATP-bound conformation indicate that the two cytoplasmic NBDs interact with each other in a head-to-tail orientation to generate two composite nucleotide binding sites. The binding and hydrolysis of ATP provides the energy required for the transport process (Hollenstein et al., 2007). Despite significant progress in the field of ABC transporters, the molecular details of the transport process are still far from being fully understood.

There is no high-resolution crystal structure available for MRP1 or any of the other 12 subfamily members, but several structures have been reported for other ABC transporters. These studies have provided a great wealth of information about structure/function relationships, revealing the drug-binding chamber and providing insight into the molecular basis of polyspecificity. The data suggest an ABC efflux transporter can exist in at least two major conformations; an “inward conformation” and an “outward conformation”. The inward conformation is the high substrate affinity state in which the binding pocket is facing towards the cytoplasm and the two NBDs are separated. The outward conformation is the low substrate affinity state with the binding pocket facing toward the extracellular space and the two NBDs closely interacting. It is not clear whether the inward conformation (with widely open NBDs) is significantly populated *in vivo*. It is possible that physiological concentrations of nucleotide (several mM) would maintain the NBDs in a closed conformation, and the amplitude of the conformational change may be smaller than is suggested by the extreme states captured by the crystal structures (Aller et al., 2009).

Molecular Pharmacology Fast Forward. Published on April 29, 2015 as DOI: 10.1124/mol.114.096792
This article has not been copyedited and formatted. The final version may differ from this version.

Moreover, based on the complexity of the transport process, the large range of substrate sizes and the diversity of ABC proteins, it is likely that additional structural substates/intermediates exist besides the two conformations revealed by the available crystal structures (Choudhury et al., 2014; Du et al., 2014; Jin et al., 2012; Kerr et al., 2010; Korkhov et al., 2012; Srinivasan et al., 2014). Electron paramagnetic resonance (EPR) and double electron-electron resonance (DEER) spectroscopy have been used to probe the conformational dynamics of ABC transporters (Joseph et al., 2014; Mishra et al., 2014; Rice et al., 2013; Schultz et al., 2011a; Schultz et al., 2011b; Sippach et al., 2014; Zou and McHaourab, 2010). One study determined that the histidine ABC transporter sampled open, semi-open. and closed conformations (Sippach et al., 2014). The closed conformation of the NBDs was only achieved in the presence of the ligand. Another study used DEER to probe conformational changes of the transport for the *E. coli* vitamin B12 ABC importer BtuCD-F. Both substrate and ATP were required for the closure of the cytoplasmic gate (Joseph et al., 2014). Furthermore, structural changes of the antigen-processing protein (TAP), detected by fluorescence resonance energy transfer (FRET), revealed that substrate is required for the complete NBD closure (Geng et al., 2013). Finally, association/dissociation of MsbA NBDs studied by luminescence resonance energy transfer revealed that the NBDs separate completely after each hydrolysis cycle (Cooper and Altenberg, 2013).

To investigate the dynamics of the human MRP1 transporter under physiological conditions in the native membrane of a living cell, we engineered a “2-color MRP1” construct with fluorescent protein tags fused to the C-terminal side of NBD1 and NBD2 (Fig. 1). We predicted that changes in MRP1 conformation would result in changes in the distance between the GFP donor and the TagRFP acceptor, altering efficiency of intramolecular FRET. Specifically, a conformational change that brings the nucleotide binding domains closer together was expected to increase

Molecular Pharmacology Fast Forward. Published on April 29, 2015 as DOI: 10.1124/mol.114.096792
This article has not been copyedited and formatted. The final version may differ from this version.

FRET from a basal level to a new higher level, reflecting the closer proximity of the fluorescent tags. We have previously used this approach to monitor structural dynamics of a calcium transporter within the native environment of the cell membrane (Hou et al., 2012; Pallikkuth et al., 2013). This strategy may be of general utility for investigating the conformational changes of transporter proteins in the native environment of the live cell.

Molecular Pharmacology Fast Forward. Published on April 29, 2015 as DOI: 10.1124/mol.114.096792
This article has not been copyedited and formatted. The final version may differ from this version.

Materials and Methods

Materials

Nucleotides, ATP analogs, doxorubicin, anti-MRP1 antibody, epigallocatechin gallate, mesalamine, calcipotriol, meropenem, benzamidine, phenylmethylsulfonyl fluoride, dithiothreitol, creatine kinase, poly-D-lysine, saponin and 2-mercaptoethanol were purchased from Sigma. [6,7- ^{3}H]$E_2$17βG (45 Ci mmol $^{-1}$) was purchased from PerkinElmer. $E_2$17βG, creatine phosphate and sodium orthovanadate were from Santa Cruz. MK571 was received from Cayman Chemicals and bismaleimidohexane (BMH) was from Pierce. Restriction enzymes were purchased from New England Biolabs and phosphate-buffered saline was purchased from Thermo Scientific.

Engineering 2-color MRP1

Using pTagRFP-N vector as a backbone, we generated a 2-color human MRP1 construct. First, C-terminal 2 kb fragment of MRP1 encoding amino acids 874-1531 (stop codon removed) was generated using primers: *forward*, 5' GTA CCG CGG CAG GAG CAG GAT GCA GAG GAG AAC 3' ; *reverse*, 5' GTA ACC GGT CT CAC CAA GCC GGC GTC TTT GGC CAT G 3' and cloned in frame with TagRFP. Engineered restriction sites are underlined. In the second step, 0.7 kb fragment encoding GFP produced using primers: *forward*, 5' GTA GTC GAC ATG GTG AGC AAG GGC GAG GAG 3' ; *reverse*, 5' GTA CCG CGG CTT GTA CAG CTC GTC CAT GCC 3' was fused to the construct. Finally, N-terminal 2.6 kb fragment of MRP1 encoding amino acids 1-873 generated with primers: *forward*, 5' CTA GAG CTC ATG GCG CTC CGG GGC TTC TGC 3' ; *reverse*, 5' GTA GTC GAC CTC TGT GCT GGC ATA GGT ACG CAG GAA 3' was ligated in frame with GFP to produce the final construct. The integrity of the

Molecular Pharmacology Fast Forward. Published on April 29, 2015 as DOI: 10.1124/mol.114.096792
This article has not been copyedited and formatted. The final version may differ from this version.

sequence was confirmed by sequencing. In the final 2-color MRP1 recombinant protein construct, the intra sequence GFP is flanked by two amino acid linkers on the N-terminus (Val-Asp) and C-terminus (Pro-Arg). The stop codon of MRP1 was removed and TagRFP was fused to the C-terminal end of MRP1 with a five amino acid linker (Thr-Gly-Leu-Ala-Thr). The schematic diagram of 2-color MRP1 is shown in Fig. 1A. Positions of GFP and TagRFP insertion were chosen to reflect the movements of NBDs and were guided by available crystal structures and sequence alignment analysis. Closure of the NBDs was predicted to result in a change from a low-FRET state to a high-FRET state. The other major consideration in the design was to avoid regions critical for the expression and function of MRP1.

MRP1-Expressing Stable Cell Line

2-color MRP1 expression vector was transfected into AAV-293 cells (Agilent, Santa Clara, CA) using jetprime transfection reagent (VWR) according to the manufacturer's instructions. After 24 hr, standard medium was replaced with medium containing G418 (400 ug/ml). Cells were maintained under G418 selection for two weeks. Then, the G418 amount was increased to 800 ug/ml. GFP expressing cells were sorted from the non-expressing cells using flow cytometry and maintained under G418 selection of 200 ug/ml.

Cell culture, Immunoblots and Fluorescence Microscopy

MRP1 expression vectors were transiently transfected into AAV-293 cells using jetprime transfection reagent according to the manufacturer's instructions. MRP1 proteins were detected by immunoblot analysis using the mouse monoclonal anti-MRP1 antibody (dilution 1:5,000). Primary antibody binding was visualized by enhanced chemiluminescence detection using goat

anti-mouse horseradish peroxidase conjugated secondary antibody (dilution 1: 10,000). Fluorescence microscopy of AAV-293 cells expressing 2-color MRP1 was performed in glass-bottom chambered coverslips (Matek Corporation, Ashland, MA) coated with poly-D-lysine 24-36 hours post-transfection with jetprime mammalian transfection kit. Fluorescent images were collected using a Nikon inverted microscope (TE 2000-U) equipped with a 60X oil objective. Widefield lamp excitation was used for FRET measurements, using computer-controlled filter wheels, as previously described (Bidwell et al., 2011; Ha et al., 2011; Hou et al., 2008; Hou and Robia, 2010; Kelly et al., 2008; Song et al., 2011). To determine the effect of substrate and/or ATP on MRP1 structure, cells were permeabilized for 2 minute in 50 µg/ml saponin in phosphate-buffered saline (PBS). Saponin permeabilization provides access for small molecules in the bath and provides control over the intracellular concentration of ATP and other impermeant species (Abrol et al., 2014; Bidwell et al., 2011; Hou et al., 2012). The saponin-containing buffer was removed and cells were rinsed once with PBS, followed by solution replacement with PBS containing substrate and/or ATP replacing endogenous nucleotides that diffuse out of the cells into the large volume in the bath.

Confocal microscopy was performed using a Leica SP5 confocal microscope equipped with a 1.3 N.A. 63 X water-immersion objective. Excitation was accomplished with Ar laser illumination at 488 nm for GFP and Doxorubicin (DOX), with emission bands of 496–533 nm for GFP and 565–650 for DOX. Total internal reflection fluorescence (TIRF) microscopy was performed with a Nikon inverted microscope (Ti-e) equipped with a 100X oil-immersion objective with (N.A. = 1.49) and a cooled CCD camera (iXon 887, Andor Technology). Through-objective TIRF excitation was achieved with a 488 nm Ar laser (for GFP). The laser incident angle was adjusted

Molecular Pharmacology Fast Forward. Published on April 29, 2015 as DOI: 10.1124/mol.114.096792
This article has not been copyedited and formatted. The final version may differ from this version.

to create an evanescent field that illuminated the plasma membrane in contact with the surface substrate. Fluorescence recovery after photobleaching (FRAP) was performed as previously described (Bossuyt et al., 2011; Robia et al., 2007). For spatially resolved photobleaching, the Ar laser 488 nm line was selected by a laser line filter and directed to the sample with a 10/90 beam splitter. The bleach beam was focused to a 1.3 μm target region on the specimen using a Keplerian telescope composed of 2 planoconvex lenses. Laser photobleaching exposure time was controlled by a Uniblitz shutter and was 100 ms. Filter transitions and shutter events were automated to provided reproducible timing. Image data were quantified with Metamorph analysis software.

Transport of ^{3}H-E$_2$17βG by MRP1 enriched Membrane Vesicles

Wild-type and 2-color MRP1 expression vectors were transfected into AAV-293 cells (at 50-70% confluency). After 48 h, the cells were harvested, and membrane vesicles were prepared as described previously (Iram and Cole, 2013). The total protein content of the vesicles was quantified using a Bio-Rad Bradford assay with bovine serum albumin as a standard. ATP-dependent transport of [^{3}H]E$_2$17βG into the inside-out membrane vesicles was measured by a rapid filtration technique (Loe et al., 1996). In brief, 10 μg of membrane vesicle protein was incubated with 400 nM/120 nCi [^{3}H]E$_2$17βG for 1 min at 37 °C in a 100 μl reaction mixture containing 10 mM $MgCl_2$ and 4 mM AMP or 4 mM ATP in transport buffer (250 mM sucrose and 50 mM Tris-HCl, pH 7.4). Reactions were stopped by dilution in ice-cold transport buffer, followed by filtration through glass fiber filters. Filters were washed with the transport buffer and radioactivity associated with the vesicles was determined. ATP-dependent uptake was calculated by subtracting the uptake in the presence of AMP from the uptake measured in the

Molecular Pharmacology Fast Forward. Published on April 29, 2015 as DOI: 10.1124/mol.114.096792
This article has not been copyedited and formatted. The final version may differ from this version.

presence of ATP. Transport assays were carried out in triplicate, and results were expressed as means ± S.D. and corrected for any differences in expression of MRP1.

FRET Measurement

FRET was quantified from cells attached to polylysine coated glass coverslip chamber dishes as previously described (Bidwell et al., 2011; Hou et al., 2012; Hou and Robia, 2010) using the E-FRET acceptor sensitization method (Zal and Gascoigne, 2004). Fluorescent images were analyzed using MetaMorph software, with fluorescence intensities quantified on a cell by cell basis. FRET efficiency (E) was calculated according to the relationship

$$E = \frac{I_{DA} - a(I_{AA}) - d(I_{DD})}{I_{DA} - a(I_{AA}) + (G - d)(I_{DD})}$$

where I_{DD} is the intensity of fluorescence emission detected in the donor channel (520/28 nm) with excitation of 480/17 nm; I_{AA} is acceptor channel (617/73 nm) emission with excitation of 556/20 nm; I_{DA} is the ‘‘FRET’’ channel, with 617/73 nm emission and excitation of 480/17 nm; a and d are cross-talk coefficients determined from acceptor-only or donor-only samples, respectively. We obtained values of d =0.165 (for GFP) and a= 0.047 (for TagRFP). G is the ratio of the sensitized emission to the corresponding amount of donor recovery, which was 1.82 for this setup. Probe separation distance (R) was calculated from the relationship described by Forster, $R = (R_0)[(1/E)-1)^{1/6}$, where E is the measured FRET value and R_0 is the Forster radius, which is 58.3 Å for the GFP-TagRFP pair. This distance calculation includes the widely used assumption of random relative orientation of the donor and acceptor fluorescence dipoles (κ^2 = 2/3). Failure of this assumption would alter the quantitative value of the distance calculated, but is not expected to alter the biological conclusions of this study, which are drawn from relative

Molecular Pharmacology Fast Forward. Published on April 29, 2015 as DOI: 10.1124/mol.114.096792
This article has not been copyedited and formatted. The final version may differ from this version.

changes in FRET. The reported FRET efficiency value represents the mean of FRET efficiencies obtained from 75 to 125 cells. For comparison of FRET with protein expression level, we quantified cell-by-cell TagRFP fluorescence (in arbitrary units) as an index of MRP1 expression. All error bars represent mean ± (SE).

High-Throughput Screening

Cells were transfected using 293fectin (Invitrogen) and G418 (Sigma) selection was used to select stable cell lines over a period of 2-3 weeks. Fifteen cell lines expressing 2-color MRP1 were further selected by fluorescence microscopy and flow cytometry. The optimal cell line was >98% positive for GFP fluorescence measured by flow cytometry. Screening of the National Clinical Collection (NCC, a library of drug-like compounds) was performed as previously described (Gruber et al., 2014). The NIH Clinical Collection (NCC, 446 compounds) is a library of unique compounds that is ideal for small-scale trial screens. The compounds are potential drug candidates that have been used in human clinical trials and are well-defined with respect to safety profile, molecular weight, and chemical properties. All compounds were dissolved in DMSO, and DMSO was present in all control wells. Cells stably expressing 2-color MRP1 were removed from a 225 cm^2 flask by incubating with TrypLE (Invitrogen) for 5 min. Cells were collected and pelleted by centrifuging at 500 x *g* for 5 min, followed by resuspension in 10 mL PBS. Cell density was determined using a Countess cell counter (Invitrogen), and cells were diluted to $1x10^6$ cells/mL. 49 µL of the cell solutions was plated by hand into a 384 well plate containing NCC compounds using a 12-channel multi-pipet. Assay plates were spun for 1 min at 200 x g and allowed to incubate at room temperature for 20 min before reading on a NovaFluor fluorescence lifetime plate reader (Fluorescence Innovations, Inc., Minneapolis, MN). GFP

Molecular Pharmacology Fast Forward. Published on April 29, 2015 as DOI: 10.1124/mol.114.096792
This article has not been copyedited and formatted. The final version may differ from this version.

fluorescence was excited with a 473 nm microchip laser from Concepts Research Corporation (Belgium, WI) and emission was filtered with 490 nm long pass and 520/35 nm band pass filters from Semrock (Rochester, NY). Time-resolved fluorescence waveforms for each well were fitted to single-exponential decays (single lifetime model) using least squares minimization global analysis software (Fluorescence Innovations, Inc.) Compounds that did not possess intrinsic fluorescence and that changed the fluorescence lifetime by more than three standard deviations were identified as hits. Dose-response assays were obtained for 4 of the eight NCC library compounds identified as hits. Each compound was obtained from Sigma Chemical Co., prepared at 10 mM in DMSO, then further diluted in DMSO to the appropriate working concentration. Each compound was plated in three wells of a 384-well plate, cells were added and the 2-color MRP1 fluorescence lifetime was quantified as described above. We measured Z' values for each of the four assay plates included in this study, as described in the HTS Assay Guidance Manual. Our data for GFP alone (donor only) comes from a screen of GFP-SERCA2a of the same NCC library on the same day as the first NCC screen of 2C-MRP1. The Z' values for each plate were >0.5 (average=0.64), exceeding the NIH-recommended standard of 0.4. We also measured the coeffient of variance (CV) for the control wells on each plate to assess instrument precision and ensure the cells had been plated uniformly. Inclusion criteria was a CV <1.5% for each plate, and average CV for the four NCC assay plates was 1.1%.

To determine whether MRP1 function was altered by hit compounds identified in the high-throughput screen, we measured DOX extrusion in MRP1-expressing cells. 5 hours after plating on glass bottom chambered coverslips, transiently-transfected cells were preincubated for 15 min with 10 μM candidate compound, then 2 μM DOX was added for 1 hr. Cells were imaged by confocal microscopy and the red fluorescence in the nucleus was quantified as an index of the

Molecular Pharmacology Fast Forward. Published on April 29, 2015 as DOI: 10.1124/mol.114.096792
This article has not been copyedited and formatted. The final version may differ from this version.

amount of DOX accumulated in the nucleus. Cells expressing MRP1 were compared to untransfected cells in the same microscopic field. Approximately 100 transfected and 100 untransfected cells were quantified for each compound. Comparisons between transfected cells and untransfected cells and between different compounds were evaluated by one way ANOVA, with Sidak's multiple comparisons test.

Results and Discussion

Expression, Localization and FRET of 2-color MRP1

To investigate the structural dynamics of MRP1 in its native membrane environment, we engineered a 2-color MRP1 construct by fusing GFP and TagRFP at the C-terminus of NBD1 and NBD2 respectively (Fig. 1A), and quantified FRET changes as an index of NBD conformational changes. MRP1 expression was verified by immunoblot analysis using cell lysates of AAV-293 cells transfected with cDNA expression vectors encoding wild-type or 2-color MRP1, loading 10 μg of protein per lane. The recombinant MRP1 protein migrated more slowly than the untagged MRP1 and produced a band at the expected molecular weight of ~ 250 kDa (Fig. 1C). Another band of lower mobility was also detected, possibly the result of protein aggregation during SDS-PAGE sample preparation. However, no aggregation was apparent in intact cells. 2-color MRP1 showed the expected plasma membrane localization by widefield fluorescence microscopy (Fig. 1D) and total internal reflection fluorescence microscopy (TIRF) (Fig. 1E), with no bright puncta or other non-uniformities. Another likely possibility is that the multiple bands represent differential denaturation of the unboiled MRP1 protein. In particular, we have frequently observed that fluorescent protein fusion tags are resistant to SDS and show mixed populations of denatured and undenatured species with different PAGE mobilities.

Molecular Pharmacology Fast Forward. Published on April 29, 2015 as DOI: 10.1124/mol.114.096792
This article has not been copyedited and formatted. The final version may differ from this version.

Fluorescence recovery after photobleaching (FRAP) showed that 2-color MRP1 protein was readily diffusible in the plasma membrane with an apparent diffusion coefficient of 4.4×10^{-3} $\mu m^2/s$ (Fig. 1F). This value is comparable to diffusion coefficients reported for a related ABC transporter CFTR, as measured by FRAP (1.7×10^{-3} $\mu m^2/s$), image correlation spectroscopy (6.3×10^{-3} $\mu m^2/s$) (Bates et al., 2006) and single particle tracking (4.0×10^{-3} $\mu m^2/s$) (Jin et al., 2007). In permeabilized AAV-293 cells transiently transfected with 2-color MRP1, we observed ~17% FRET efficiency irrespective of protein expression levels (Fig. 1G). The lack of concentration dependence is consistent with intramolecular FRET (Hou et al., 2012) with little apparent contribution of non-specific energy transfer (Ha et al., 2011) or other intermolecular FRET. Although we cannot formally rule out the possibility of formation of MRP1 oligomers, the data suggest that the oligomeric status of MRP1 remained the same over the range of protein concentration used in these experiments.

MRP1 Transport Activity in Membrane Vesicles and Live Cells

To determine if the engineered 2-color MRP1 was functional, the vesicular transport activity was measured using a prototypical MRP1 substrate, $E_2$17βG. Inside-out membrane vesicles prepared from AAV-293 cells transiently transfected with wild-type or 2-color MRP1 were used to determine the uptake of this organic anion. 2-color MRP1 membrane vesicles exhibited similar levels of [^{3}H]$E_2$17βG uptake as those of wild-type MRP1 membrane vesicles (Fig. 2A). Results were comparable to other reports (Iram and Cole, 2012; Iram and Cole, 2013).

2-color MRP1 transport activity was also evaluated in live cells by measuring extrusion of the fluorescent anticancer drug doxorubicin, a well-known substrate of MRP1. Confocal microscopy

Molecular Pharmacology Fast Forward. Published on April 29, 2015 as DOI: 10.1124/mol.114.096792
This article has not been copyedited and formatted. The final version may differ from this version.

of AAV-293 cells showed doxorubicin accumulating in the nucleus of untransfected cells (Fig. 2B, red), but doxorubicin fluorescence was not observed in cells expressing 2-color MRP1 (Fig. 2B, green). These results indicate that the 2-color MRP1 trafficked properly to the plasma membrane and was functionally active as an efflux pump. MRP1-dependent doxorubicin efflux was blocked by the known MRP1 inhibitor MK571 and by BMH, a cell permeable cross-linker (Rajagopal and Simon, 2003)(Fig. 2B). The present results are not consistent with a previous study that showed intracellular localization of MRP1. That report suggested that drug transporters MRP1, P-gp, and BCRP do not reduce the overall accumulation of doxorubicin within the cell, but rather confer multidrug resistance by sequestering the drug in intracellular vesicles, sparing the nucleus (Rajagopal and Simon, 2003). Here we see clear and uniform expression of 2-color MRP1 mostly at the plasma membrane (Fig. 2B, green). These data are consistent with a model in which ABC drug transporters such as MRP1, P-gp and BCRP function as plasma membrane efflux pumps, conferring multidrug resistance by reducing the intracellular accumulation of the drug (Aller et al., 2009; Iram and Cole, 2013).

MRP1 Conformational Changes

To measure ligand-dependent conformational changes of MRP1 protein, we performed FRET microscopy of saponin-permeabilized (Jamur and Oliver, 2010; Ruggiero et al., 1985; Wassler et al., 1987) cells, which provided control over the concentration of nucleotide and transportable substrates by washing out the endogenous contents, including the nucleotides. First, the effect of ATP binding on NBDs conformation was investigated by measuring FRET changes at different ATP concentrations. As seen in Fig. 3A, FRET increased with ATP in a concentration-dependent manner to a maximum FRET of 25% at 1mM ATP. The final value was similar to that measured

Molecular Pharmacology Fast Forward. Published on April 29, 2015 as DOI: 10.1124/mol.114.096792
This article has not been copyedited and formatted. The final version may differ from this version.

in intact (unpermeabilized) cells. The data suggest that ATP binding induces closure of the MRP1 cytoplasmic domains, bringing opposing NBDs into close proximity. A hyperbolic fit to the data gave an apparent ATP binding affinity of 107 μM. The ATP concentration dependence of the conformational change did not appear to be positively cooperative, though other studies have provided evidence for cooperativity of ATPase activity for MRP1 and other ABC transporters (Ramaen et al., 2006; Senior and Bhagat, 1998; Zaitseva et al., 2006). A Hill fit of the data in Fig. 3A yielded a Hill coefficient of 0.72 (error of fit 0.45). The average FRET observed for 2-color MRP1 in apo condition was 16.7 ± 1.0%, and FRET did not change significantly with the addition of the substrate ($E_2$17βG) ($p = 0.20$), suggesting that there was not a detectable conformational change in the NBDs upon substrate binding (Fig. 3B). These results are consistent with the crystal structure study, which showed that both apo and the inhibitor bound P-gp structures were almost identical (Aller et al., 2009). In contrast, the presence of 1 mM ATP alone led to a significant increase in FRET to 25.3 ± 0.6% ($p = 0.0002$ vs. Apo), consistent with a conformational change that decreased the distance between the donor and acceptor fluorescent tags. Even though substrate alone did not induce NBD closure, $E_2$17βG added in the presence of ATP increased FRET to 28.6 ± 1.3% ($p = 0.019$ vs. ATP alone) (Fig. 3B). We observed a similar response for another known MRP1 substrate LTC_4 ($p = 0.022$ vs. ATP alone). The order of addition of substrate and ATP did not affect the final FRET efficiency. Our data suggest that ATP binding induces the major conformational change and brings the two NBDs closer, however, substrate binding is required to achieve more compact, high-FRET conformation. Notably, FRET was not increased by AMP, and only modestly elevated by ADP. This is in contrast to a recent study of Pgp (Verhalen et al., 2012) that reported an incremental increase in intramolecular FRET efficiency with the addition of substrate alone.

Molecular Pharmacology Fast Forward. Published on April 29, 2015 as DOI: 10.1124/mol.114.096792
This article has not been copyedited and formatted. The final version may differ from this version.

Interpretation and Limitations of FRET Measurements:

FRET distances were calculated from the Förster relationship assuming random relative dipolar orientation ($\kappa^2 = 2/3$). Deviations from this assumption would increase or decrease the apparent probe separation distance. Moreover, the expressed fluorescent tags are large (~29 KDa), which adds uncertainty about the relative position of the tag and the underlying domain. However, our recent computational study provides support for the assumption that fluorescent proteins communicate closely with the domain to which they are attached and thus FRET changes may serve as a useful index of protein conformational changes (Smolin and Robia, 2015). Here, nonspecific FRET was not subtracted from the measured FRET values (Ha et al., 2011; Kelly et al., 2008) because there was no evidence of a concentration-dependent increase in FRET (Fig. 1G). Overall, our results indicate that the GFP and TagRFP are separated by 76.2 ± 0.9 Å in the apo condition and upon binding to ATP and ATP/substrate this distance was decreased to 69.8 ± 0.4 and 67.9 ± 0.7 Å, respectively. The apparent magnitude of the NBD movement observed here was less than would be predicted from comparison of the mouse P-gp (apo) and nucleotide-bound Sav1866 crystal structures (~20 Å difference) (Aller et al., 2009; Dawson and Locher, 2006). However, it is important to note that ensemble measurements of average FRET efficiency may overlook multiple structural subpopulations (Pallikkuth et al., 2013; Verhalen et al., 2012). Moreover, substrate binding may not induce an all-or-nothing switch to a new conformation, but rather shift the balance of an equilibrium of multiple structures. Thus, the apparent probe separation distance change of ~8 Å measured here may underestimate the true magnitude of the MRP1 conformational change.

Molecular Pharmacology Fast Forward. Published on April 29, 2015 as DOI: 10.1124/mol.114.096792
This article has not been copyedited and formatted. The final version may differ from this version.

MRP1 Interaction with ATP Analogs

Structural studies have obtained high-quality crystals by trapping ABC transporters in a pre-hydrolysis state by incubation with non-hydrolyzable ATP analogs (Dawson and Locher, 2007). Here we quantified the structural change of MRP1 in response to ATPγS, AMPPNP, and AMPPCP. All of the analogs produced a much smaller FRET increase compared to ATP (Fig. 3C). This was unexpected since these analogs are generally assumed to have a binding affinity that is as high as ATP. One possibility is that the analogs bind tightly but do not induce a significant closure of the NBDs. If so, the analogs would be expected to compete with ATP for the nucleotide binding site. However, incubation of MRP1 with 1mM of the analog did not prevent 500 μM ATP from increasing FRET to 28-29% vs. apo-MRP1 (Fig. 3D). The data suggest that ATP analogs do not prevent closure of MRP1, since they do not compete with ATP and reduce FRET. Rather, ATP analogs may bind with poor affinity to NBDs of MRP1. This interpretation is supported by the observation that higher levels of the ATP analogs (5 mM) did increase FRET (Fig. 3E) to varying degrees, all somewhat less potently than ATP. ATP analogs AMPPNP and AMPPCP in particular showed a reduced maximal FRET. It is unknown whether these nucleotide analogs stabilize the same MRP1 conformation as ATP. High-resolution crystal structures of a related bacterial transporter Sav1866 showed that AMPPNP produced an outward-facing conformation that was not grossly different from the ADP-bound structure (Dawson and Locher, 2006; Dawson and Locher, 2007).

Inhibition of MRP1 Activity

ATPases can be arrested in a post-hydrolysis state by incubation with orthovanadate under conditions permissive for ATP hydrolysis (Iram and Cole, 2011), trapping ADP at the catalytic

Molecular Pharmacology Fast Forward. Published on April 29, 2015 as DOI: 10.1124/mol.114.096792
This article has not been copyedited and formatted. The final version may differ from this version.

site (Koike et al., 2004). When orthovanadate-induced ADP trapping was performed in AAV-293 cells permeabilized with saponin, the FRET value obtained was 29.2 ± 0.7%, similar to the FRET value for the active transport condition in the presence of ATP and substrate 28.7 ± 0.9% (Fig. 3F). The data suggest that the orthovanadate-induced transition state also increases the population of molecules in the most compact conformation. The closely interacting NBDs of the ADP-trapped transporter imply that resetting of the transporter to an open (low FRET) conformation is accomplished by release of the substrate and/or ADP rather than ATP hydrolysis. A recent study (Verhalen et al., 2012) focused on P-gp NBD structural dynamics reported a significant increase in FRET upon addition of inorganic vanadate, but we observed no such effect of vanadate with MRP1. As with orthovanadate, MRP1 inhibition by MK571 caused no significant change in the average FRET efficiency (Fig. 3F) compared to the active transport condition. The data suggest that MK571 stops enzymatic cycling by stabilizing a high-FRET conformation of MRP1. This is consistent with the proposed mechanism of competitive inhibition of substrate binding by MK571 (Gekeler et al., 1995) However, crosslinking the transporter with BMH reduced intramolecular FRET from 28.7 to 22.4% (Fig. 3F). This is consistent with BMH crosslinking MRP1 in an intermediate conformation, partway between Apo (open) and ATP-bound or substrate-bound (closed) structures.

Potential Application for Drug Discovery

Previously we used a different 2-color pump, the P-type ATPase SERCA, to detect activator/inhibitor candidates in a high-throughput screen of a library of drug-like compounds (Gruber et al., 2014). The present data suggest that this approach can be successfully generalized to ABC proteins and to other families of transporters. To evaluate whether 2-color MRP1 could

Molecular Pharmacology Fast Forward. Published on April 29, 2015 as DOI: 10.1124/mol.114.096792
This article has not been copyedited and formatted. The final version may differ from this version.

be useful for identification of novel substrates or inhibitors, we performed a FRET-based screen of the National Clinical Collection (NCC) library of compounds, which are known to be biologically active. We applied test compounds to live cells in a 384 well assay format as previously described (Gruber et al., 2014) and selected hits that altered the fluorescence lifetime of the GFP donor on MRP1 in repeated screens of the library. Two independent screens identified 20 and 34 hits, respectively, with 13 hits in common between the two screens. Of the 13, 8 were in the normal range of intensity. Notably, several of these compounds are very closely structurally related (Fig. 4A); calcipotriol is an analog of calcitriol and epigallocatechin gallate is very similar to hyperoside. Fig. 4B shows that the fluorescence lifetime provided a more robust selection criterion than fluorescence intensity, with better well-to-well reproducibility and improved signal to noise ratio. We selected 4 of the 8 hits for additional characterization. Fig. 4C shows the dose response for epigallocatechin gallate (antioxidant), mesalamine (anti-inflammatory), calcipotriol (vitamin D analog), and meropenem (antibiotic). While meropenem and mesalamin produce only weak effects on donor lifetime, both epigallocatechin gallate and calcipotriol elicited large lifetime changes with sigmoidal dose dependence. Epigallocatechin gallate, in particular, showed a high apparent affinity (EC_{50} = 1.7 μM) with evidence of cooperative binding (Hill coefficient = 2.06). To test whether candidate compounds altered the transport activity of MRP1 we quantified DOX accumulation in the nuclei of HEK cells as in Fig. 2B. Representive images of cells for each treatment condition are provided in Sup. Fig. 1. Fig. 4D shows that DOX accumulation in the nuclei of cells was greatly reduced by expression of MRP1 ("+MRP1", *p = _<0.0001 vs. untransfected), but pretreatment with 1μM of the known MRP1 inhibitor MK571 decreased this extrusion activity (Fig. 4D, #p <0.0001 vs. "+MRP1"), increasing DOX fluorescence in the nucleus (Sup. Fig. 1). We could not

evaluate the effect of mesalamine because it interfered with the DOX treatment even in untransfected cells. Supplemental Fig. 1 shows that cells pretreated with mesalamine showed DOX fluorescence localized to intracellular compartments but not in the nucleus, irrespective of MRP1 expression. The reason for this interference with DOX uptake was unclear. No apparent decrease in transport activity was observed for epi. gallate or meropenem, but calcipotriol decreased MRP1 activity, increasing DOX accumulation (Fig. 4D, #p = 0.0085 vs. "+MRP1"). The data suggest that calcipitriol (Vitamin D analog) may interfere with the ability of MRP1 to transport DOX. This result is noteworthy as Vitamin D has been observed to potentiate the anti-tumor activity of DOX and other chemotherapeutic agents (Ma et al., 2010).

The data demonstrate the potential utility of MRP1 intramolecular FRET for discovery of small-molecule modulators of MRP1 structure/function. This assay offers several advantages over alternatives. Compared to transport assays (Fig. 2A,B), a FRET-based screen is simple- it does not involve addition of other compounds (like DOX) and it does not require a wash step or detailed calibration. It is also potentially sensitive to both allosteric regulators and transportable substrates, whereas an assay based on quantifying transport may not detect substrates that bind weakly or fail to compete with the test substrate. Future studies will screen larger libraries of compounds to identify additional molecules that alter MRP1 intramolecular FRET. Potential hit compounds could include transportable substrates or novel inhibitors of MRP1 activity.

Conclusions

We have engineered a 2-color MRP1 protein construct that exhibits large changes in FRET in response to binding of nucleotide, transportable substrates and inhibitory drugs. In addition to performing well in a pilot high-throughput screen of a drug library, the construct has provided

Molecular Pharmacology Fast Forward. Published on April 29, 2015 as DOI: 10.1124/mol.114.096792
This article has not been copyedited and formatted. The final version may differ from this version.

insight into the conformational changes during the transport cycle of MRP1. The data are broadly compatible with the ATP switch model (Abele and Tampe, 2004; Higgins and Linton, 2004), in which transport is driven by NBD association/dissociation in response to ATP binding and hydrolysis. However, given the uncertainties of the present ensemble FRET measurements we cannot rule out alternative models, such as constant-contact models in which the NBDs do not fully dissociate, but open enough to allow ADP/ATP exchange. Moreover, it is likely that additional conformational states exist besides the two states detected by crystallography. Nevertheless, the data suggest that intramolecular FRET is a useful index of the conformational changes of transport and underscore the utility of fluorescent protein tags as reporters of pump dynamics. They are generally benign for function (Bidwell et al., 2011; Hou et al., 2012) (Fig. 2) and can be fused to arbitrary positions with fixed stoichiometry for maximum sensitivity to the conformational change of interest. To scale this assay for high-throughput screening, 2-color transporters may be expressed in stable cell lines (Gruber et al., 2012), allowing selective retrieval of candidate compounds that are non-toxic, cell permeant, and potent for eliciting the desired conformational change. For 2-color MRP1, in particular, we envision a discovery program that may identify existing drugs not previously known to be transported by this broad spectrum drug-resistance protein. Such information may provide insight into previously unexplained drug resistance or drug interaction mechanisms. MRP1 screening may also yield novel inhibitors useful for treating chemotherapy resistance in anticancer regimens

Molecular Pharmacology Fast Forward. Published on April 29, 2015 as DOI: 10.1124/mol.114.096792
This article has not been copyedited and formatted. The final version may differ from this version.

Acknowledgements

The authors are grateful for technical assistance from Daniel J. Blackwell, Zhanjia Hou, Ryan D. Himes and Nikolai Smolin. We thank Prof. Toni Pak for assistance with radioisotope transport assays.

Molecular Pharmacology Fast Forward. Published on April 29, 2015 as DOI: 10.1124/mol.114.096792
This article has not been copyedited and formatted. The final version may differ from this version.

Authorship Contributions

Participated in research design: Iram, Robia, Thomas

Conducted experiments: Iram, Raguimova, Gruber

Contributed new reagents or analytic tools: Iram, Robia, Thomas

Performed data analysis: Iram, Robia, Gruber, Thomas, Raguimova

Wrote or contributed to the writing of the manuscript: Iram, Robia, Gruber, Thomas

References

Abele R and Tampe R (2004) The ABCs of immunology: structure and function of TAP, the transporter associated with antigen processing. *Physiology* **19**: 216-224.

Abrol N, Smolin N, Armanious G, Ceholski DK, Trieber CA, Young HS and Robia SL (2014) Phospholamban C-terminal residues are critical determinants of the structure and function of the calcium ATPase regulatory complex. *J Biol Chem* **289**(37): 25855-25866.

Aittoniemi J, Fotinou C, Craig TJ, de Wet H, Proks P and Ashcroft FM (2009) Review. SUR1: a unique ATP-binding cassette protein that functions as an ion channel regulator. *Philosophical transactions of the Royal Society of London Series B, Biological sciences* **364**(1514): 257-267.

Aller SG, Yu J, Ward A, Weng Y, Chittaboina S, Zhuo R, Harrell PM, Trinh YT, Zhang Q, Urbatsch IL and Chang G (2009) Structure of P-glycoprotein reveals a molecular basis for poly-specific drug binding. *Science* **323**(5922): 1718-1722.

Bates IR, Hebert B, Luo Y, Liao J, Bachir AI, Kolin DL, Wiseman PW and Hanrahan JW (2006) Membrane lateral diffusion and capture of CFTR within transient confinement zones. *Biophys J* **91**(3): 1046-1058.

Bidwell P, Blackwell DJ, Hou Z, Zima AV and Robia SL (2011) Phospholamban binds with differential affinity to calcium pump conformers. *J Biol Chem* **286**(40): 35044-35050.

Bossuyt J, Chang CW, Helmstadter K, Kunkel MT, Newton AC, Campbell KS, Martin JL, Bossuyt S, Robia SL and Bers DM (2011) Spatiotemporally distinct protein kinase D activation in adult cardiomyocytes in response to phenylephrine and endothelin. *J Biol Chem* **286**(38): 33390-33400.

Choudhury HG, Tong Z, Mathavan I, Li Y, Iwata S, Zirah S, Rebuffat S, van Veen HW and Beis K (2014) Structure of an antibacterial peptide ATP-binding cassette transporter in a novel outward occluded state. *Proceedings of the National Academy of Sciences of the United States of America* **111**(25): 9145-9150.

Conseil G, Deeley RG and Cole SP (2006) Functional importance of three basic residues clustered at the cytosolic interface of transmembrane helix 15 in the multidrug and organic anion transporter MRP1 (ABCC1). *J Biol Chem* **281**(1): 43-50.

Cooper RS and Altenberg GA (2013) Association/dissociation of the nucleotide-binding domains of the ATP-binding cassette protein MsbA measured during continuous hydrolysis. *J Biol Chem* **288**(29): 20785-20796.

Dawson RJ and Locher KP (2006) Structure of a bacterial multidrug ABC transporter. *Nature* **443**(7108): 180-185.

Dawson RJ and Locher KP (2007) Structure of the multidrug ABC transporter Sav1866 from Staphylococcus aureus in complex with AMP-PNP. *FEBS letters* **581**(5): 935-938.

Dean M and Allikmets R (2001) Complete characterization of the human ABC gene family. *Journal of bioenergetics and biomembranes* **33**(6): 475-479.

Deeley RG, Westlake C and Cole SP (2006) Transmembrane transport of endo- and xenobiotics by mammalian ATP-binding cassette multidrug resistance proteins. *Physiological reviews* **86**(3): 849-899.

Du D, Wang Z, James NR, Voss JE, Klimont E, Ohene-Agyei T, Venter H, Chiu W and Luisi BF (2014) Structure of the AcrAB-TolC multidrug efflux pump. *Nature* **509**(7501): 512-515.

Gekeler V, Ise W, Sanders KH, Ulrich WR and Beck J (1995) The leukotriene LTD4 receptor antagonist MK571 specifically modulates MRP associated multidrug resistance. *Biochemical and biophysical research communications* **208**(1): 345-352.

Geng J, Sivaramakrishnan S and Raghavan M (2013) Analyses of conformational states of the transporter associated with antigen processing (TAP) protein in a native cellular membrane environment. *J Biol Chem* **288**(52): 37039-37047.

Gottesman MM (2002) Mechanisms of cancer drug resistance. *Annual review of medicine* **53**: 615-627.

Gruber SJ, Cornea RL, Li J, Peterson KC, Schaaf TM, Gillispie GD, Dahl R, Zsebo KM, Robia SL and Thomas DD (2014) Discovery of enzyme modulators via high-throughput time-resolved FRET in living cells. *J Biomol Screen* **19**(2): 215-222.

Gruber SJ, Haydon S and Thomas DD (2012) Phospholamban mutants compete with wild type for SERCA binding in living cells. *Biochemical and biophysical research communications* **420**(2): 236-240.

Ha KN, Masterson LR, Hou Z, Verardi R, Walsh N, Veglia G and Robia SL (2011) Lethal Arg9Cys phospholamban mutation hinders Ca2+-ATPase regulation and phosphorylation by protein kinase A. *Proceedings of the National Academy of Sciences of the United States of America* **108**(7): 2735-2740.

Higgins CF and Linton KJ (2004) The ATP switch model for ABC transporters. *Nature structural & molecular biology* **11**(10): 918-926.

Hipfner DR, Almquist KC, Leslie EM, Gerlach JH, Grant CE, Deeley RG and Cole SP (1997) Membrane topology of the multidrug resistance protein (MRP). A study of glycosylation-site mutants reveals an extracytosolic NH2 terminus. *J Biol Chem* **272**(38): 23623-23630.

Hollenstein K, Dawson RJ and Locher KP (2007) Structure and mechanism of ABC transporter proteins. *Current opinion in structural biology* **17**(4): 412-418.

Hou Z, Hu Z, Blackwell DJ, Miller TD, Thomas DD and Robia SL (2012) 2-Color calcium pump reveals closure of the cytoplasmic headpiece with calcium binding. *PloS one* **7**(7): e40369.

Hou Z, Kelly EM and Robia SL (2008) Phosphomimetic mutations increase phospholamban oligomerization and alter the structure of its regulatory complex. *J Biol Chem* **283**(43): 28996-29003.

Hou Z and Robia SL (2010) Relative affinity of calcium pump isoforms for phospholamban quantified by fluorescence resonance energy transfer. *J Mol Biol* **402**(1): 210-216.

Iram SH and Cole SP (2011) Expression and function of human MRP1 (ABCC1) is dependent on amino acids in cytoplasmic loop 5 and its interface with nucleotide binding domain 2. *J Biol Chem* **286**(9): 7202-7213.

Iram SH and Cole SP (2012) Mutation of Glu521 or Glu535 in cytoplasmic loop 5 causes differential misfolding in multiple domains of multidrug and organic anion transporter MRP1 (ABCC1). *J Biol Chem* **287**(10): 7543-7555.

Iram SH and Cole SP (2013) Differential functional rescue of Lys and Lys processing mutants of MRP1 (ABCC1) by chemical chaperones reveals different domain-domain interactions of the transporter. *Biochimica et biophysica acta* **1838**(3): 756-765.

Jamur MC and Oliver C (2010) Permeabilization of cell membranes. *Methods in molecular biology* **588**: 63-66.

Jin MS, Oldham ML, Zhang Q and Chen J (2012) Crystal structure of the multidrug transporter P-glycoprotein from Caenorhabditis elegans. *Nature* **490**(7421): 566-569.

Jin S, Haggie PM and Verkman AS (2007) Single-particle tracking of membrane protein diffusion in a potential: simulation, detection, and application to confined diffusion of CFTR Cl- channels. *Biophys J* **93**(3): 1079-1088.

Joseph B, Korkhov VM, Yulikov M, Jeschke G and Bordignon E (2014) Conformational cycle of the vitamin B12 ABC importer in liposomes detected by double electron-electron resonance (DEER). *J Biol Chem* **289**(6): 3176-3185.

Kelly EM, Hou Z, Bossuyt J, Bers DM and Robia SL (2008) Phospholamban oligomerization, quaternary structure, and sarco(endo)plasmic reticulum calcium ATPase binding measured by fluorescence resonance energy transfer in living cells. *J Biol Chem* **283**(18): 12202-12211.

Kerr ID, Jones PM and George AM (2010) Multidrug efflux pumps: the structures of prokaryotic ATP-binding cassette transporter efflux pumps and implications for our understanding of eukaryotic P-glycoproteins and homologues. *The FEBS journal* **277**(3): 550-563.

Koike K, Conseil G, Leslie EM, Deeley RG and Cole SP (2004) Identification of proline residues in the core cytoplasmic and transmembrane regions of multidrug resistance protein 1 (MRP1/ABCC1) important for transport function, substrate specificity, and nucleotide interactions. *J Biol Chem* **279**(13): 12325-12336.

Korkhov VM, Mireku SA and Locher KP (2012) Structure of AMP-PNP-bound vitamin B12 transporter BtuCD-F. *Nature* **490**(7420): 367-372.

Loe DW, Almquist KC, Deeley RG and Cole SP (1996) Multidrug resistance protein (MRP)-mediated transport of leukotriene C4 and chemotherapeutic agents in membrane vesicles. Demonstration of glutathione-dependent vincristine transport. *J Biol Chem* **271**(16): 9675-9682.

Ma Y, Trump DL and Johnson CS (2010) Vitamin D in combination cancer treatment. *Journal of Cancer* **1**: 101-107.

Mishra S, Verhalen B, Stein RA, Wen PC, Tajkhorshid E and McHaourab HS (2014) Conformational dynamics of the nucleotide binding domains and the power stroke of a heterodimeric ABC transporter. *eLife* **3**: e02740.

Pallikkuth S, Blackwell DJ, Hu Z, Hou Z, Zieman DT, Svensson B, Thomas DD and Robia SL (2013) Phosphorylated phospholamban stabilizes a compact conformation of the cardiac calcium-ATPase. *Biophys J* **105**(8): 1812-1821.

Rajagopal A and Simon SM (2003) Subcellular localization and activity of multidrug resistance proteins. *Molecular biology of the cell* **14**(8): 3389-3399.

Ramaen O, Leulliot N, Sizun C, Ulryck N, Pamlard O, Lallemand JY, Tilbeurgh H and Jacquet E (2006) Structure of the human multidrug resistance protein 1 nucleotide binding domain 1 bound to Mg2+/ATP reveals a non-productive catalytic site. *J Mol Biol* **359**(4): 940-949.

Rice AJ, Alvarez FJ, Schultz KM, Klug CS, Davidson AL and Pinkett HW (2013) EPR spectroscopy of MolB2C2-a reveals mechanism of transport for a bacterial type II molybdate importer. *J Biol Chem* **288**(29): 21228-21235.

Robia SL, Campbell KS, Kelly EM, Hou Z, Winters DL and Thomas DD (2007) Forster transfer recovery reveals that phospholamban exchanges slowly from pentamers but rapidly from the SERCA regulatory complex. *Circ Res* **101**(11): 1123-1129.

Ruggiero M, Zimmerman TP and Lapetina EG (1985) ATP depletion in human platelets caused by permeabilization with saponin does not prevent serotonin secretion induced by collagen. *Biochemical and biophysical research communications* **131**(2): 620-627.

Schultz KM, Merten JA and Klug CS (2011a) Characterization of the E506Q and H537A dysfunctional mutants in the E. coli ABC transporter MsbA. *Biochemistry* **50**(18): 3599-3608.

Schultz KM, Merten JA and Klug CS (2011b) Effects of the L511P and D512G mutations on the Escherichia coli ABC transporter MsbA. *Biochemistry* **50**(13): 2594-2602.

Senior AE and Bhagat S (1998) P-glycoprotein shows strong catalytic cooperativity between the two nucleotide sites. *Biochemistry* **37**(3): 831-836.

Sheppard DN and Welsh MJ (1999) Structure and function of the CFTR chloride channel. *Physiological reviews* **79**(1 Suppl): S23-45.

Sippach M, Weidlich D, Klose D, Abe C, Klare J, Schneider E and Steinhoff HJ (2014) Conformational changes of the histidine ATP-binding cassette transporter studied by double electron-electron resonance spectroscopy. *Biochimica et biophysica acta* **1838**(7): 1760-1768.

Smolin N and Robia SL (2015) A structural mechanism for calcium transporter headpiece closure. *The journal of physical chemistry B* **119**(4): 1407-1415.

Song Q, Pallikkuth S, Bossuyt J, Bers DM and Robia SL (2011) Phosphomimetic mutations enhance oligomerization of phospholemman and modulate its interaction with the Na/K-ATPase. *J Biol Chem* **286**(11): 9120-9126.

Srinivasan V, Pierik AJ and Lill R (2014) Crystal structures of nucleotide-free and glutathione-bound mitochondrial ABC transporter Atm1. *Science* **343**(6175): 1137-1140.

Verhalen B, Ernst S, Borsch M and Wilkens S (2012) Dynamic ligand-induced conformational rearrangements in P-glycoprotein as probed by fluorescence resonance energy transfer spectroscopy. *J Biol Chem* **287**(2): 1112-1127.

Wassler M, Jonasson I, Persson R and Fries E (1987) Differential permeabilization of membranes by saponin treatment of isolated rat hepatocytes. Release of secretory proteins. *The Biochemical journal* **247**(2): 407-415.

Zaitseva J, Oswald C, Jumpertz T, Jenewein S, Wiedenmann A, Holland IB and Schmitt L (2006) A structural analysis of asymmetry required for catalytic activity of an ABC-ATPase domain dimer. *The EMBO journal* **25**(14): 3432-3443.

Zal T and Gascoigne NR (2004) Photobleaching-corrected FRET efficiency imaging of live cells. *Biophys J* **86**(6): 3923-3939.

Zou P and McHaourab HS (2010) Increased sensitivity and extended range of distance measurements in spin-labeled membrane proteins: Q-band double electron-electron resonance and nanoscale bilayers. *Biophys J* **98**(6): L18-20.

Molecular Pharmacology Fast Forward. Published on April 29, 2015 as DOI: 10.1124/mol.114.096792
This article has not been copyedited and formatted. The final version may differ from this version.

Footnotes:

Financial Support: This work was supported by National Institutes of Health grants to S.L.R. [HL106189, HL092321] and D.D.T. [GM27906], and by a gift from the McCormick Foundation to Loyola University Chicago.

Reprint Requests: Seth L. Robia, Department of Cell and Molecular Physiology, Stritch School of Medicine, Loyola University Chicago, 2160 South First Avenue, Maywood, IL 60153, Tel: (708) 216-2522, E-mail: srobia@luc.edu

Molecular Pharmacology Fast Forward. Published on April 29, 2015 as DOI: 10.1124/mol.114.096792
This article has not been copyedited and formatted. The final version may differ from this version.

Figure Legends

Figure 1. Expression, localization and FRET of 2-color MRP1. **(**A) Schematic diagram of 2-color MRP1 construct showing an intrasequence GFP (two amino acid linker on each side) and a C-terminus TagRFP (five amino acid linker). (B) Crystal structure of mouse P-gp in apo condition showing the separated NBDs (left) (Aller et al., 2009); crystal structure of nucleotide-bound *S. aureus* Sav1866 showing the closed NBD structure (right) (Dawson and Locher, 2006). (C) Immunoblots of whole cell lysates (10 μg) containing wild-type (WT-MRP1) and 2-color MRP1 (2C-MRP1) compared to untransfected cells (control), with detection by mouse monoclonal anti-MRP1 (1:5000 dilution, 1 hr at room temperature) or anti-GFP antibody (1: 2000 dilution, 1 hr at room temperature). (D) AAV-293 cells expressing 2-color MRP1 were plated on glass-bottom chambered coverslips as described in experimental procedues. Fluorescent images were collected using a Nikon inverted microscope equipped with a 60X objective. Widefield lamp excitation and computer controlled filter wheels were used to acquire GFP and TagRFP images. (E) MRP1 membrane expression and lateral diffusion investigated by TIRF microscopy and FRAP of a 1.3 μm target region. (F) Data from FRAP were analyzed using a non-linear curve fit with a single exponential function. ***G***, MRP-1 FRET did not depend on protein expression level.

Figure 2. Functional characterization of 2-color MRP1. (A) ATP-dependent uptake of [^{3}H]$E_2$17βG by the membrane vesicles. Membrane vesicles were incubated with substrate and transport reaction was allowed for 1 min at 37 °C. Values are mean ± SD for triplicate determinations in a single experiment; both WT and 2-color MRP1 values were significantly different from control ($p<0.05$). Similar results were obtained in a second experiment with

vesicles derived from independent transfection. (B) AAV-293 cells (control) and 2-color MRP1 expressing cells were exposed to 10 μM doxorubicin (DOX) for 15 min . DOX containing media was replaced with PBS and cells were imaged using a confocal microscope equipped with 63X objective. DOX and GFP were excited at 488 nm wavelength using Ar laser, with emission bands of 565-650 for DOX and 496-533 nm for GFP. DOX was detected by red fluorescence and was mostly localized in the nucleus, 2-color MRP1 (green) showed plasma membrane localization. To inhibit MRP1 activity, cells were incubated with MK571 (50 μM) or BMH (1 mM) for 15 min before DOX treatment.

Figure 3. Dynamic FRET changes of 2-color MRP1 in permeabilized AAV-293 cells. FRET measurements were made as described in the experimental procedures. Cells plated on glass-bottom chambered coverslips were permeabilized for 2 minute at room temperature in 50 μg/ml saponin in PBS which washed out the endogenous cell contents including the nucleotides. PBS buffer supplemented with 5 mM $MgCl_2$ was used in all FRET experiments. All incubations (10-15 min) and FRET measurements were made at room temperature. (A) FRET increased with ATP. (B) MRP1 FRET response to nucleotide and transportable substrates $E_2$17βG or LTC_4. (C) MRP1 interaction with ATP analogs applied at 1 mM concentration. (D) Competition of 1 mM nucleotide analogs with 500 μM ATP. Analogs did not prevent ATP from increasing MRP1 FRET. (E) ATP analogs increased MRP1 FRET when applied at high concentration. (F) The effect of inhibitors of MRP1 including 1 mM vanadate, 50 μM MK571, 1 mM BMH. Except for the apo condition, 1 mM ATP + 50 μM $E_2$17βG were added to each. ATP, ATP+ $E_2$17βG, ATP+LTC_4, and ADP values were statistically significant vs. Apo ($p<0.05$).

Molecular Pharmacology Fast Forward. Published on April 29, 2015 as DOI: 10.1124/mol.114.096792
This article has not been copyedited and formatted. The final version may differ from this version.

Figure 4. High-throughput screening with 2-color MRP1. (A) Hits from the National Clinical Collection. (B) We observed significantly less variability and improved signal to noise with screening with 2-color MRP1 on the basis of fluorescence lifetime compared to fluorescence intensity. (C) Dose response for select hit compounds. Epigallocatechin gallate showed the highest apparent affinity (EC_{50} = 1.7 μM). (D) DOX uptake into the nucleus of HEK cells after pretreatment with candidate compounds. Values are mean nuclear fluorescence ± SE, normalized to untransfected cells in the same microscopic field. The red horizontal line indicates a high level of DOX accumulation (as in untransfected cells), the green line indicates decreased accumulation of DOX suggesting drug efflux by MRP1.

Molecular Pharmacology Fast Forward. Published on April 29, 2015 as DOI: 10.1124/mol.114.096792
This article has not been copyedited and formatted. The final version may differ from this version.

Fig-1

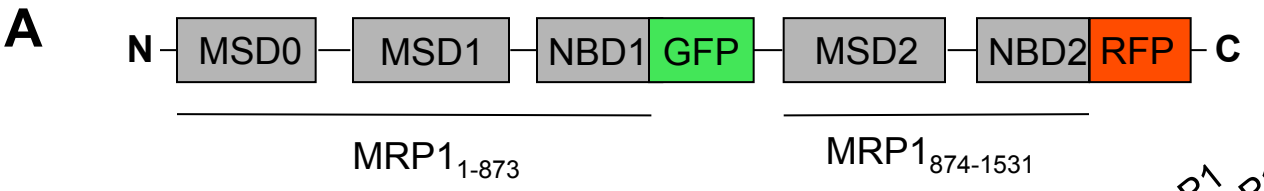

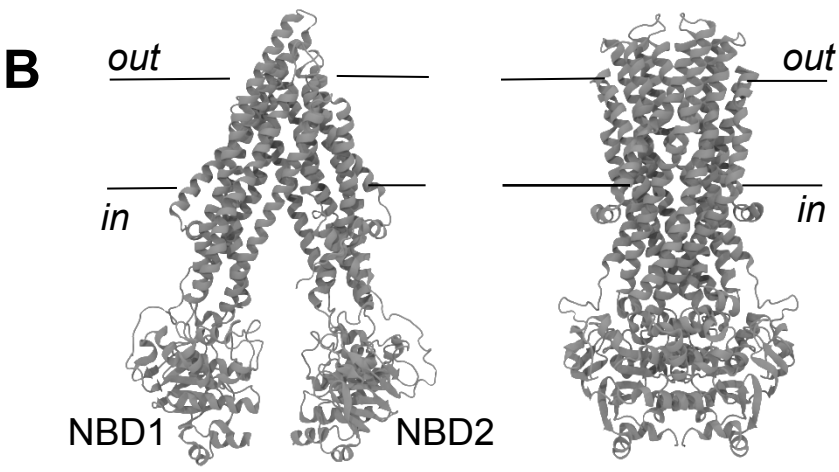

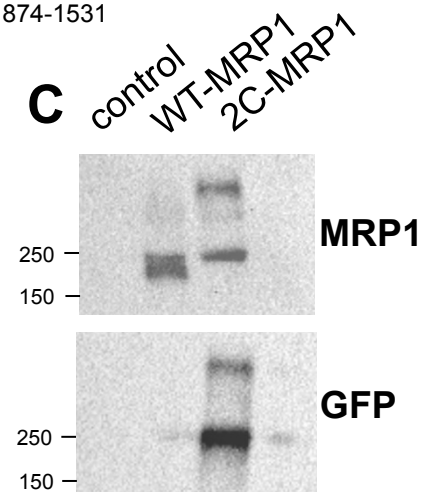

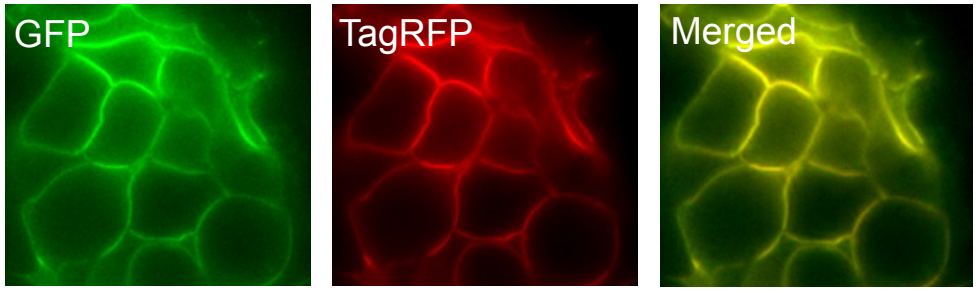

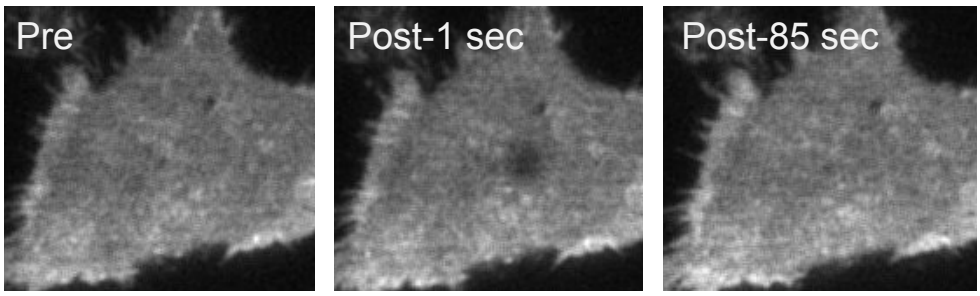

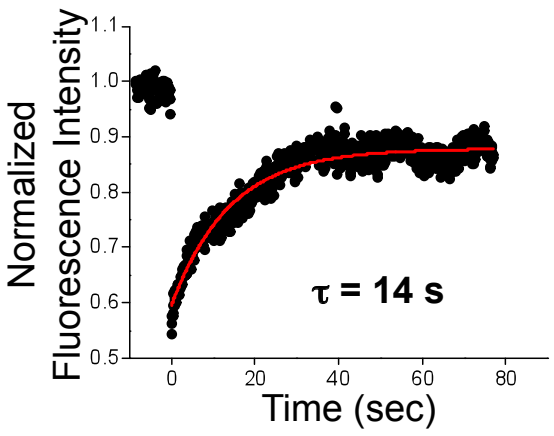

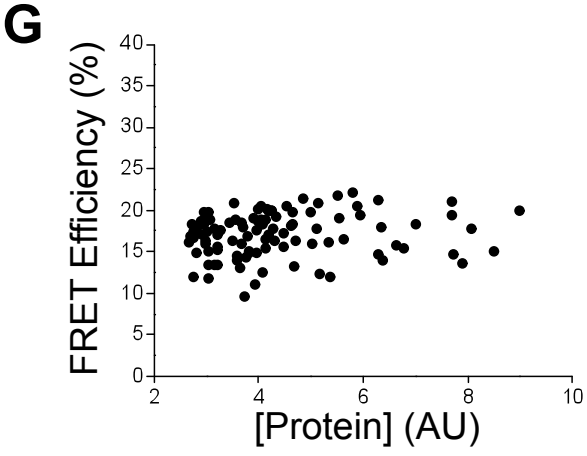

Molecular Pharmacology Fast Forward. Published on April 29, 2015 as DOI: 10.1124/mol.114.096792
This article has not been copyedited and formatted. The final version may differ from this version.

Fig-2

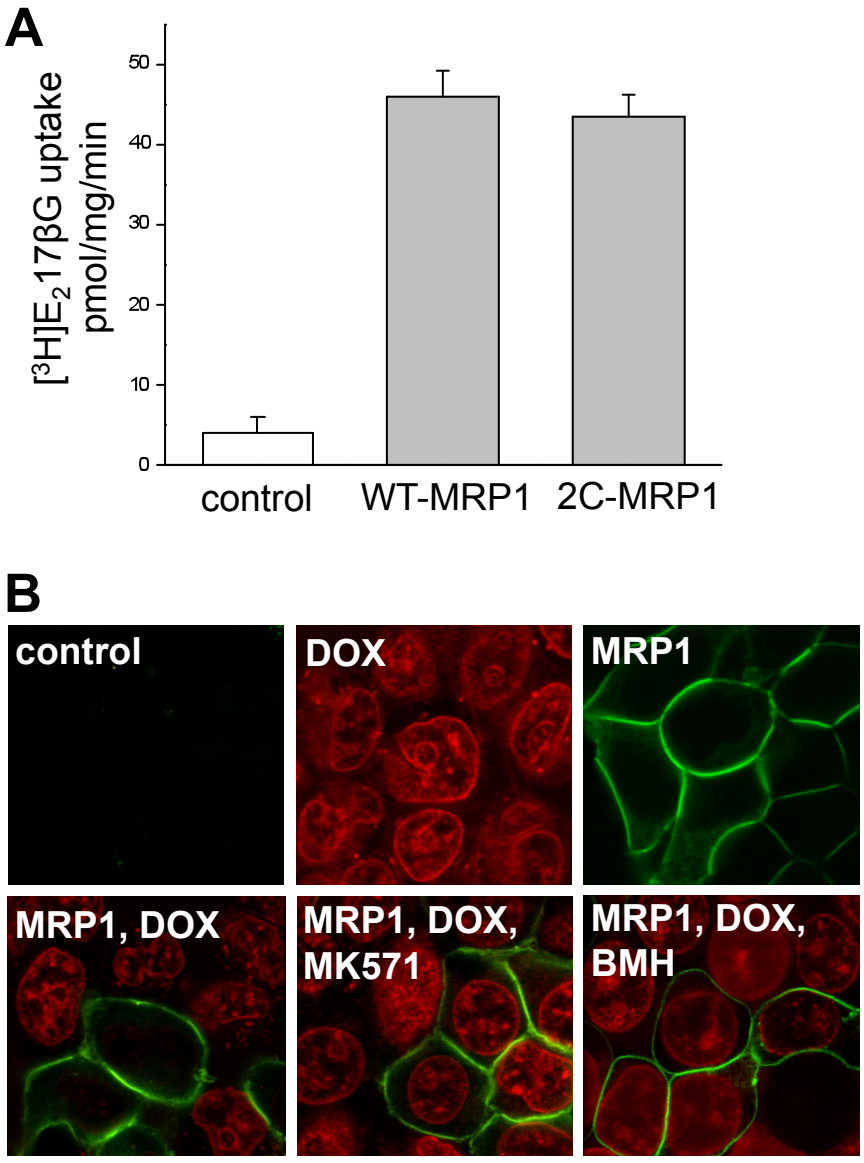

Molecular Pharmacology Fast Forward. Published on April 29, 2015 as DOI: 10.1124/mol.114.096792
This article has not been copyedited and formatted. The final version may differ from this version.

Fig-3

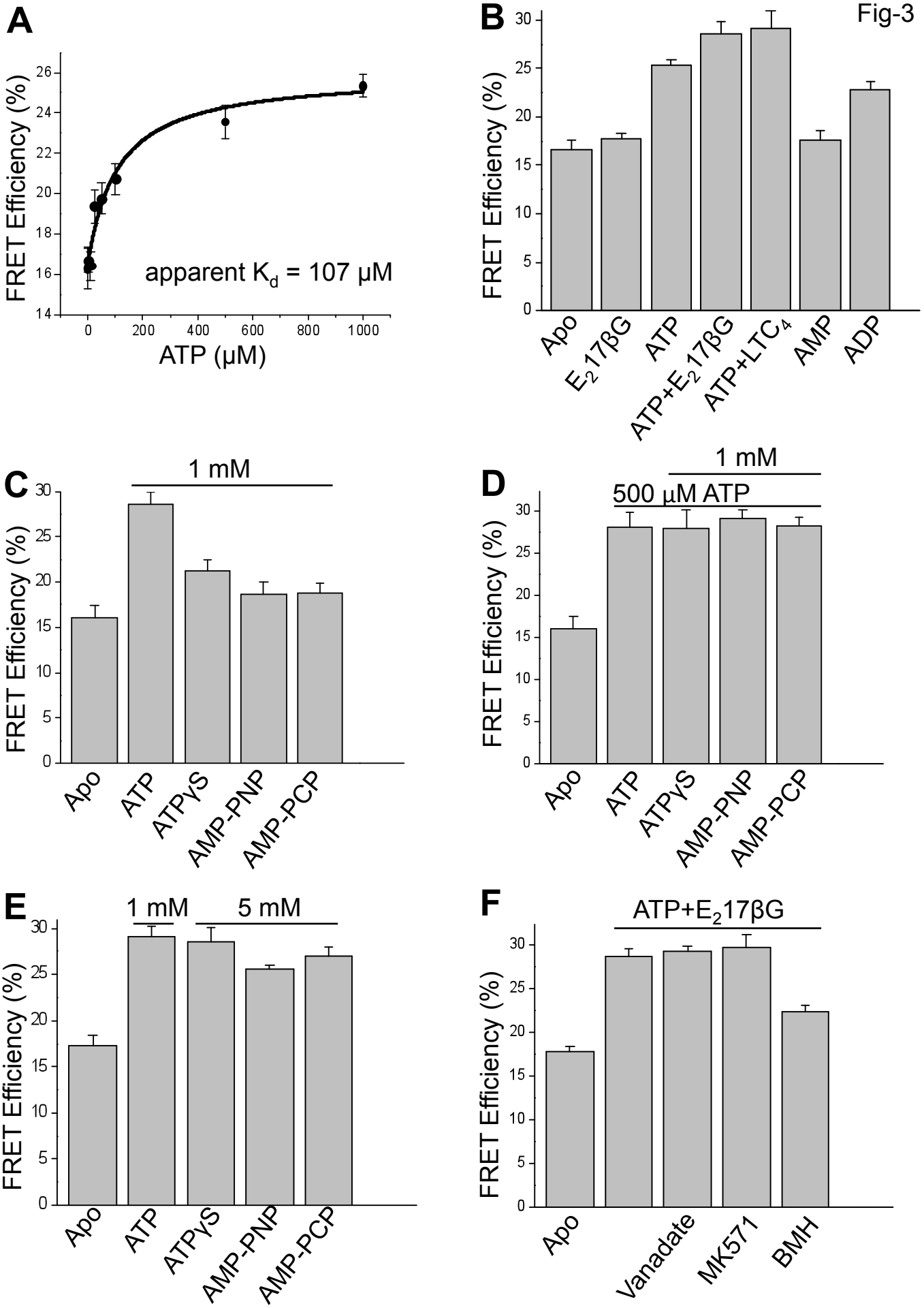

Molecular Pharmacology Fast Forward. Published on April 29, 2015 as DOI: 10.1124/mol.114.096792
This article has not been copyedited and formatted. The final version may differ from this version.

Fig-4